Lab 3
Stellar Observing with CCDs: Noise Regimes and Point Spread Functions
ASTR 329

James Hartwick

Nov 26, 2014

1 Objective

To study the properties of CCDs while under real observing conditions, and to answer the question "how does the uncertainty in the measurement of the brightness of a star depend on the star brightness itself?"

2 Introduction

Photometric observations are a method for quantifying the information received from astronomical objects. The observed photon flux and approximate distance to the object can be used to determine it's luminosity, temperature, and size. This experiment will introduce the process photometric and noise analysis by performing it on ten stars in the open star cluster NGC 6819.

Photon noise can be shown to be Poisson noise which is simply the square root of the signal. This is not the only source of error which must be taken into account for CCDs as this experiment will show. Scintillation noise is a time dependent error which arises from atmospheric turbulence. This turbulence can refract the incident photons which affects the number of photons received across the detector.

Further correctors must be made to remove other sources of photons which do not originate from the object of interest. The Point Spread Function (PSF) of other nearby stars may overlap onto the observed object causing an increase in flux. Although stars are essentially point sources due to their distance we cannot resolve them as such due to physical limitations. This flux distribution we observe is called the PSF of the star. Furthermore the night time sky brightness must be corrected for as well.

3 Procedure

3.1 Observations

Science, flat, and bias frames were taken of NGC 6819 using the 0.8m telescope in the Bob Wright Building Observatory.

4 Reductions and Discussion

4.1 Bias Subtraction and Flat Fielding

All reduction and analysis were done using a Python script created using the imported modules SciPy, PyFits, PyRaf, and MatPlotLib. The bias frames were combined and averaged to create a master bias frame. This will be subtracted from all science and flat field frames. The median of the flat frames was then taken to create a master flat frame. The master bias was then subtracted from the science and master flat frames. Finally the science frame was divided by the master flat and re-normalized.

4.2 Aperture Photometry

The PyRaf *daophot* function was then used on 10 stars selected from the data. *daophot* performs aperture photometry which is the process of measuring all flux within a given radius about an objects center. An estimated value for the sky flux level must be subtracted as well. In order to find this a circular annulus around the object is used. A inner annulus radius of 40 was used with a width of 25. Multiple aperture sizes were attempted, and a size of 12 was deemed best after comparing the results of daophot across all science images. The standard deviation of the mean of the results was used to compare aperture sizes as well the the results of other students.

Table 1. Shows the output from daophot aperture photometry. Sum represents the (object+sky) signal value, Flux is the object signal, and sky is the product of Msky and Area (Aperture scaling.)

4.3 RMS Uncertainties

The RMS uncertainty is given by:

$$\sigma \;=\; \sqrt{\Sigma(x-\bar{x})^2}$$

Both x and $\bar{x}$ values come from Table 1. where $\bar{x}$ is derived from the average of the values. The values for the Star and Sky signal RMS for each star were calculated in this manner. To calculate the object RMS the root of the squares of the (object+sky) RMS and sky RMS were calculated. This method may be used because the flux is calculated by combinations of the sky level and the

Table 1.

Star Location	Sum(counts)	Msky(counts)	Area(pixels)	Flux(counts)	Sky(counts)
877, 1127	176220.43	1256.82	78.82	108543.94	99057.58
1005, 1201	106948.48	1152.3	72.24	43870.65	83241.83
1125, 996	735544.38	1257.02	78.77	666906.64	99016.1
633, 841	3468643.45	1256.89	78.82	3400404.64	99072.46
1294, 1144	246758.92	1257.04	78.78	178688.84	99028.25
1300, 1306	74570.83	1257.14	78.75	6417.72	99004
1230, 1300	232028.75	1256.98	78.78	163824.13	99025.05
791, 743	274999.65	1256.75	78.85	207812.83	99090.36
444, 1106	101644.13	1256.97	78.79	35256.69	99033.87
1574, 1457	296682.09	1256.81	78.81	228872.19	99048.16

(object+sky) combined level. A second value for the object RMS was calculated using the quadratic method to demonstrate consistency between the two methods. These results are tabulated in Table 2 below.

Table 2.

Star Location	σ_s	σ_{os}	σ_o	σ_o (Quadratic Method)
877, 1127	11076.7550	224483.1687	360186.7656	360357.0460
1005, 1201	21283.3416	13176.5658	33149.1913	39393.5212
1125, 996	11296.3681	18299.1891	18333.5175	21534.2935
633, 841	10720.3297	74660.3379	69235.5070	70060.5517
1294, 1144	11516.3120	6306.2488	11472.6705	16255.6947
1300, 1306	11323.1760	598.1693	11492.7033	16133.7083
1230, 1300	11318.8446	5644.4250	11453.5205	16102.7754
791, 743	11142.5241	6337.9915	11662.2545	16129.6009
444, 1106	10468.0972	1537.5693	10315.4242	14696.5654
1574, 1457	11498.8916	5959.2318	11435.7548	16217.3054

4.4 Plots of σ vs log(s) for raw observations

Plots were created for raw observation RMS vs the logarithm of the corresponding signal.

Photons obey Poisson statistics and thus they follow a relation of $\sigma \alpha \sqrt{S}$ in the region where Poisson noise is dominant.

Figure 1 plots the Sky RMS uncertainty vs the log(Sky signal). It is dominated by a single data point. When this point is removed there appears to be an upward trend which is consistent with expectations, but not much confidence should be put on this result.

Figure 2 plots the Object + Sky RMS uncertainty vs log(Object+Sky signal). Again a single point dominates and when it is removed an upwards trend is observed. This time the trend is much more clear and regimes can be identified. First the Poisson noise regime for lower signal levels, then as signal increase, the slope does as well. This is due to another noise component known as scintillation noise which will be discussed later in this report.

The condition S = ft may be violated when there is strong turbulence or short exposure times. If strong turbulence is present the incoming flux would not be constant due to changes in the refractive index of the atmosphere. For short exposure times the random nature of the incident photons would be too great to guarantee any kind of definite relation.

4.5 Relations Between Signal and Noise

Figure 3 plots the Log(Object RMS Noise) vs Log(Object Signal). This log-log plot is used to identify the power relation between N and S. With the exception of two data points a clear linear relation is observed between the two. The slope is greater than 0.5 which is what one would expect for Poisson statistics so clearly there are more noise components. This may be accounted for by scintillation noise. Figure 3 also arguably demonstrates the greater effect of scintillation noise as signal increases. The slope appears to increase slightly at higher signal compared to lower signal. There are not enough data points to make this point with too much confidence however.

Figure 4 plots the Log(Object Signal to Noise Ratio) vs Log(Object Signal). With the exception of two data points this plot shows a flattening slope at higher signal levels. This is due to the effects of scintillation. N becomes more closely related to S as scintillation noise becomes more dominant at higher signal levels. Thus the curve flattens out as signal increases.

4.6 Sky Brightness

The stars with ID's 13, 26, 91 correspond to the locations (791, 743), (1300,1306), (1294, 1144) respectively. These stars have had there magnitudes previously identified and listed in the lab manual[1]. The sky brightness may be determined using these values and following equation:

$M_{sky} = M_{star} - 2.5log(\frac{Star\ counts}{Sky\ counts} - 2.5log(\frac{(1'')^2}{(0.436'')^2}))$
for the 2048x2048CCD and:

$M_{sky} = M_{star} - 2.5log(\frac{Star\ counts}{Sky\ counts} - 2.5log(\frac{(1'')^2}{(0.869'')^2}))$
for the 0.5m telescope CCD.

4.7 Scintillation Noise

Scintillation noise comes from the perturbations in the refractive index of the atmosphere along the path between the source and the detector. These perturbations cause the light to travel along different paths through the atmosphere. The effects of scintillation noise are shown in Figure 4 where, as signal increases, the signal to noise ratio stars relatively constant with a slope less than 0.5. Because of this slope we can conclude that the noise is increasing faster than just Poisson noise. The other component to this is the scintillation noise.

For fainter stars scintillation is not observed because, as shown in Figure 4, Poisson noise dominates for lower signal levels. Less signal corresponds to few perturbations and thus less scintillation effects.
In non-photometric conditions the atmospheric extinction becomes a function of the air mass between the source and the detector. Thus their effects could appear as fluctuations in the signal in a similar manner to scintillation noise. Flat fielding attempts to remove the pixel to pixel variations intrinsic to each CCD. If these variations were unaccounted for the signal would fluctuate spatially in a non uniform way similar to scintillation noise. Especially if observations are taken over a long period of time. Therefor observations which do not flat field correct my appear to have scintillation noise.

4.8 Multiple Stars on a Single CCD Frame

The best way to approximate the PSF is by using the brightest stars in the frames because it will be the least affected by background noise. Therefore it is easiest to acquire a best fit for the PSF from these brighter sources. Once this PSF is subtracted from the frame fainter stars can then be revealed behind it. The less dominant the background noise the smaller the residual will be after PSF subtraction thus yielding the best results.

5 Conclusion

The effects of scintillation noise as signal increases was demonstrated. Brighter sources are dominated by scintillation which flattens out the S/N vs S relation. When multiple objects appear in the same frame it was explained that it is best to use the PSF of the brightest star as a basis for the fainter stars due to the lesser effects of background noise on it. This background noise becomes dominant for fainter stars so their PSF should not be used as a basis for others.

Note: some aspects of this lab were not completed. I attempted to do my data analysis with PyRaf which seemed to mostly work, but I had many issues which I was not able to remedy in time. I should have used IRAF, but I thought this would be fun to try. As such I wouldn't put much confidence in any of the results from this experiment even though many of the results did agree with theory when certain data points were removed.

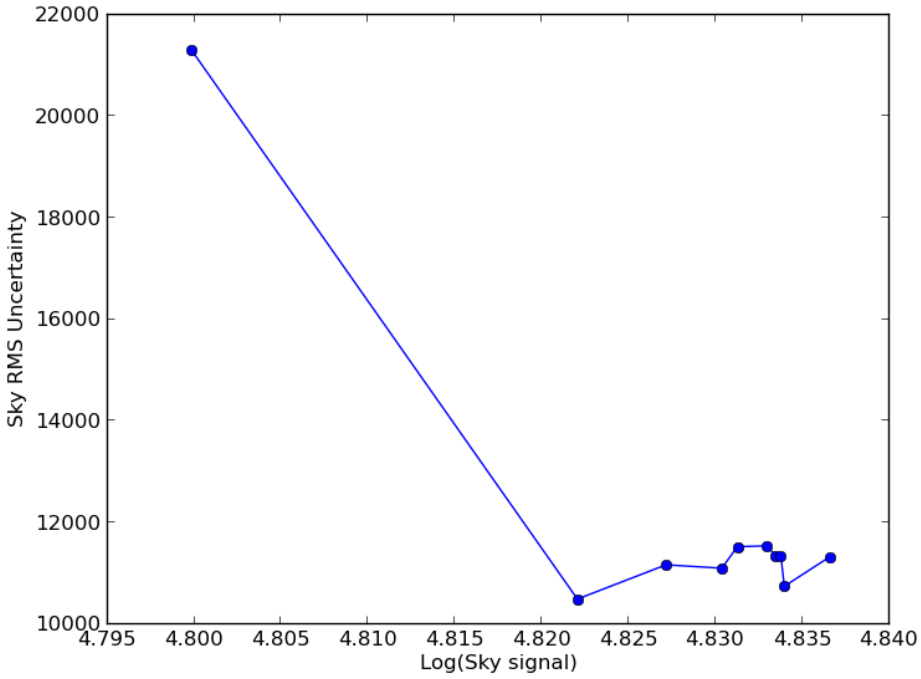

Figure 1: Sky RMS Uncertainty vs Log(Sky signal)

6 References

1. Stephenson Yang, Astr 329 Lab 3 Notes.

7 Figures

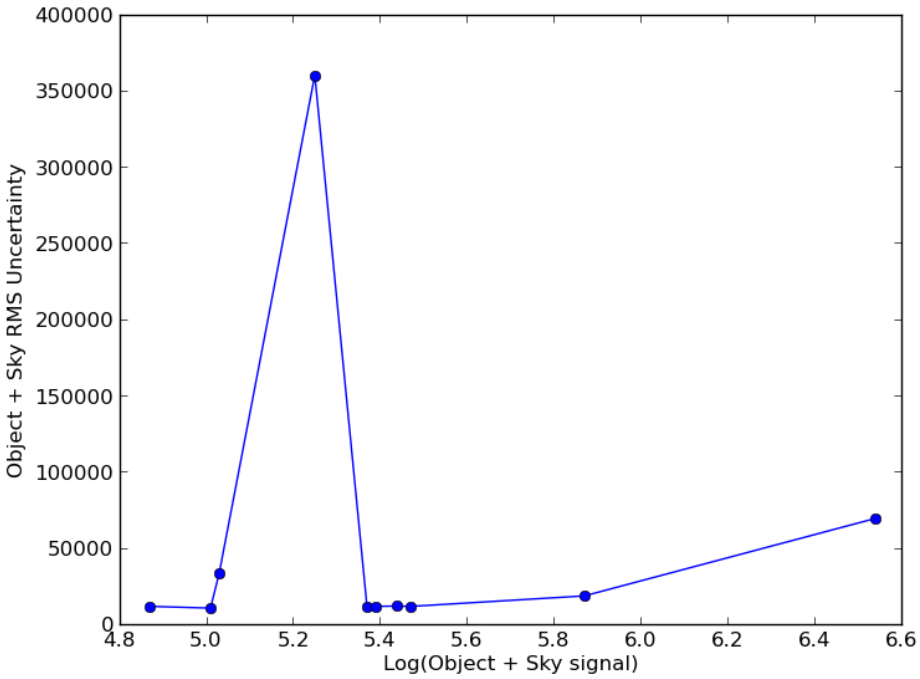

Figure 2: Object+Sky RMS Uncertainty vs Log(Object+Sky signal)

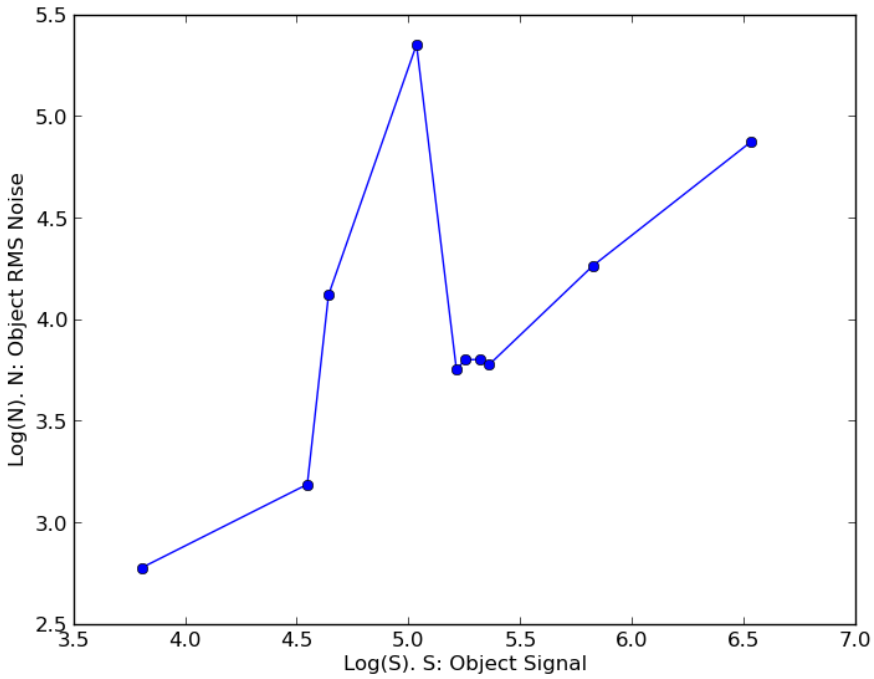

Figure 3: Log(Object RMS Noise) vs Log(Object Signal)

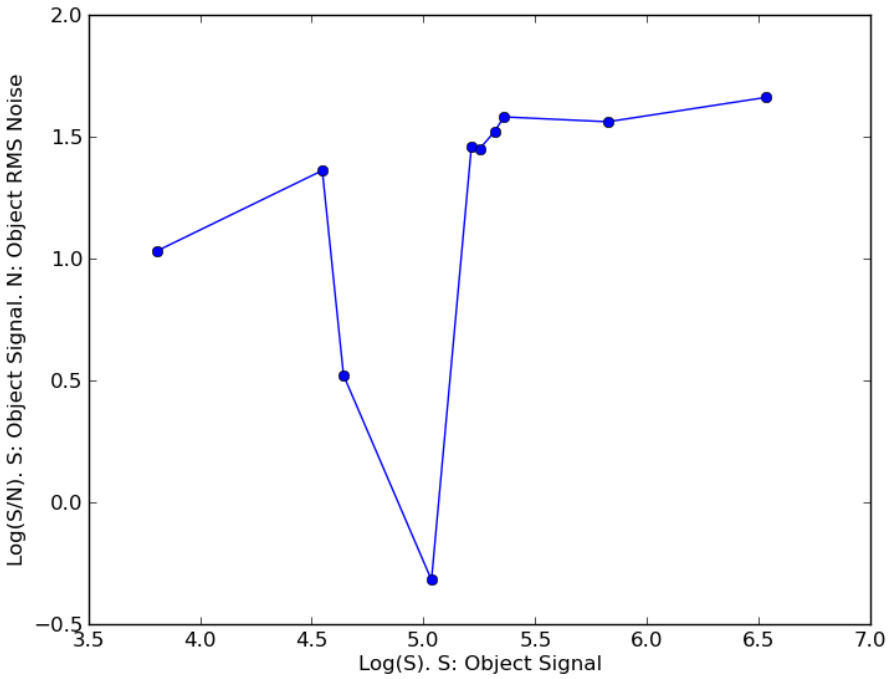

Figure 4: Log(Object Signal to Noise Ratio) vs Log(Object Signal)